

ECOLOGICAL MAPPING WITH GEOSPATIAL FOUNDATION MODELS

Craig Mahlasi¹ , Gciniwe S. Baloyi¹ , Zaheed Gaffoor¹ , Levente Klein¹ , Anne Jones¹ , Etienne Vos¹ , Michal Muszynski² , Geoffrey Dawson¹ , and Campbell Watson¹ 

¹*IBM Research*; ²*IBM Sustainability Software*

Abstract—Geospatial foundation models (GFM) are a fast-emerging paradigm for various geospatial tasks, such as ecological mapping. However, the utility of GFM has not been fully explored for high-value use cases. This study aims to explore the utility, challenges and opportunities associated with the application of GFM for ecological uses. In this regard, we fine-tune several pretrained AI models, namely, Prithvi-EO-2.0 and TerraMind, across three use cases, and compare this with a baseline ResNet-101 model. Firstly, we demonstrate TerraMind’s LULC generation capabilities. Lastly, we explore the utility of the GFM in forest functional trait mapping and peatlands detection. In all experiments, the GFM outperform the baseline ResNet models. In general TerraMind marginally outperforms Prithvi. However, with additional modalities TerraMind significantly outperforms the baseline ResNet and Prithvi models. Nonetheless, consideration should be given to the divergence of input data from pretrained modalities. We note that these models would benefit from higher resolution and more accurate labels, especially for use cases where pixel-level dynamics need to be mapped.

Index Terms—Peatlands, Forest classification, TerraMind, Prithvi

I. INTRODUCTION

Geospatial foundation models (GFM) are a fast-emerging area within the field of artificial intelligence (AI) models. The aim of these models is to learn robust and generalizable representations of the physical environment that can be adapted to a wide range of downstream tasks and applications while reducing the amount of labelled data needed. Most notable examples of GFM include [1–8]. While these models have shown value in general purpose downstream applications including general land cover mapping, segmentation of spectrally distinct features and non-complex scenario object-detection, these applications can be understood as being trivial. Conversely, ecological applications of GFM are often not straightforward. This is because the intricate characteristics of the Earth’s biodiversity are not directly measured by earth-observing satellites or other data used in the pretraining of GFM [9]. Even with fine-tuning, several limitations including low domain generalization, geographic bias and temporal bias have been observed [10–12]. For these reasons, task-specific machine learning supervised models remain a mainstay for ecological and conservation applications.

In this paper, we explore the utility of GFM for ecological mapping tasks. We do not seek to conduct a survey of GFM,

their capabilities and advances, for this we refer readers to [10–16]. We focus on the utility, challenges and opportunities associated with developing high fidelity models for ecological applications using GFM. To this end, we start by considering zero-shot land use land cover (LULC) mapping performance using a generative GFM. Secondly, we assess the performance of GFM on specialized downstream tasks including forest trait mapping and peatland detection. Finally, we consider input data distribution shifts, label quality as well as the practicalities of multimodal foundation models.

II. METHODS

A. Study sites and use cases

1) *NEON sites*: The National Science Foundation’s National Ecological Observatory Network (NEON) sites are a network of ecologically important field sites located across the United States [17]. Long-term ecological data are collected from these sites, including characteristics of plant and animal life, soil, nutrients, freshwater and atmospheric dynamics, with the aim of better understanding the impact of climate change on biodiversity. Here we explore the usefulness of GFM performing forest trait mapping across the NEON sites, focusing on leaf form and canopy cover density segmentation.

2) *Karukinka Nature Park*: Karukinka Nature Park, located in southern Patagonia on the archipelago of Tierra del Fuego, is a world-renowned ecological hotspot [18]. This region contains extensive and well developed peat bogs, which contribute significantly to global carbon sequestration [19]. The formation of the peatlands is driven by the presence of *Sphagnum Magellanicum*, a peat moss common in the region. From an aerial perspective, this species of peat moss commonly appears reddish-brown coloured. Here we explore the utility of GFM to delineate and monitor peatland extent.

B. Models

In this work, we use two GFM and one pretrained deep learning model: Prithvi-EO-2.0 [1], TerraMind [2], and ResNet-101 [20]. Both Prithvi and TerraMind are transformer-based GFM developed specifically for and pretrained using Earth Observation data, whereas ResNet is a convolution-based model pretrained on RGB images collected online and spanning thousands of categories. TerraMind is

designed to operate over and generate multimodal Earth Observation representations, enabling joint reasoning across heterogeneous geospatial inputs. We consider ResNet a strong baseline due to its inductive bias and robust performance in limited-data regimes. Model training and fine-tuning were performed using TerraTorch, a toolkit built for GFM fine-tuning and benchmarking [21]. TerraTorch is built on PyTorch Lightning and therefore inherits PyTorch Lightning's training, validation, and testing framework through low-code YAML configuration files.

C. Input modalities

For each NEON site, Copernicus Sentinel-2 L2A (S2-L2A) [22] cloud free composites were generated for the summer months (May - August) of 2019. While for the Karukinka study area, S2-L2A cloud free composites were generated for the summer months (October to March) of 2018-2019. For the multimodal experiments, the RGB and NDVI modalities were computed from the S2-L2A cloud free composites. For experiments that include Copernicus Sentinel-1 GRD (S1-GRD) [23] modality, monthly mosaics for IW variant in the VV and VH decibel gamma bands for January - March 2019 where collected. Thereafter the mean of VV and VH bands where computed across the three months. For the DEM modality, the Copernicus GLO-30 Digital Surface Model where collected for the various study sites [24]. The PEATGRIDS-NDVI approach utilised S2-L2A cloud free composites, which were computed for each of the five global peatland locations. All modalities were regrid and aligned to the resolution (10m) and coordinate reference system of S2-L2A dataset. Finally, the data (inputs and labels) were split into patches of size 224 x 224 pixels.

D. Deriving labels

1) *Forest traits mapping*: The Copernicus Land Monitoring Service Global Dynamic Land Cover data provide yearly global estimates of LULC across 23 classes from 2015-2019 at 100m resolution [25]. This LULC dataset contains 12 forest categories that classify forests based on three criteria, namely canopy density, leaf form, and leaf retention. For leaf form segmentation, the forest categories were extracted and merged into 5 classes: needle leaf forests, broad leaf forests, mixed leaf forests, unknown leaf form forests, and other (non-forested). While for canopy density, the 12 forest classes where merged into three broad categories, classifying open forest (canopy cover is between 15-70%), closed forest (canopy cover is >70%), and other (non-forested).

2) *Peatlands detection*: Several datasets were adapted to derive a total of three unique label datasets that roughly define the extent of the peatlands in the study area. The first dataset is the Copernicus Land Monitoring Service Global Dynamic Land Cover for 2020 [26] (henceforth, this shall be known as COP 2020 LULC) which provides classifications for 11 land cover classes at a 10m resolution.

Here, the herbaceous vegetation and herbaceous wetland classes are extracted, which appear to overlap well with the presence of peat moss. Thereafter, to eliminate false labels on mountain tops and steeply dipping slopes, all labels above an elevation of 450m and a slope angle above 10°, were removed. The second dataset is the Chilean National Forestry Corporation (CONAF) inventory of native vegetation resources dataset which classifies vegetation land cover for the entire Chile [27]. Here, we extract the peat bog class (turbales in Spanish) as labels. The third and final dataset is the PEATGRIDS dataset which contains peat thickness and carbon stock maps estimated over peatland areas across the globe at 1×1km resolution [28]. The PEATGRIDS data is sampled at five geographically distinct peatlands across the world: Karukinka, Chile; Ontario, Canada; Luginetskiy, Russia; Zhytomir Oblast, Ukraine; Louisiana, USA. It is further processed with NDVI computed from the S2-L2A cloud free composites at each location. A threshold of 0.23 - 0.8 [29, 30] is applied to the NDVI layers to produce a binary mask classifying peat from non-peat, and the labels defined at the intersection of the PEATGRIDS positive labels and the NDVI positive labels.

E. Experiments

1) *TerraMind generation*: The mapping of ecological processes often requires timely updates of data (such as earth observation data) and the outputs derived from the said data. However, sub-optimal acquisition conditions and long revisit times often hinder the application of earth observation data in ecological mapping. With the TerraMind model, however, this data limitation can be partially addressed through the "any-to-any" modality generation feature, where any of the input modes can be used to generate or translate into any of the other modes, thereby, filling in the data gaps. Here, we test TerraMind's zero-shot capability in generating ESRI LULC modality based on the S2-L2A modality and evaluate it against the original ESRI global 10-class land cover dataset [31].

2) *Forest traits mapping*: To assess the utility of GFMs on forest traits mapping, two tasks were chosen: leaf form and canopy cover density segmentation. The experiments focus on the NEON sites described in section II-A1. S2-L2A cloud free composites were used as inputs. We fine-tune Prithvi, TerraMind, and ResNet on a single A100-80GB GPU. The AdamW optimizer was used with a learning rate of 1×10^{-4} , the dice loss function and a weight decay configuration of 5×10^{-2} were specified.

3) *Peatland detection*: Here, we fine-tune TerraMind, Prithvi and ResNet models with all three label datasets (section II-D2) to segment the peatlands from the surrounding land cover types. For Prithvi and ResNet, only unimodal fine-tuning experiments where conducted using 12 S2-L2A bands. For TerraMind, both unimodal (S2-L2A) and multimodal (S1-GRD, S2-L2A, RGB, NDVI and DEM) fine-tuning

experiments where conducted. All fine-tuning experiment where run on single A100-80GB GPU where the AdamW optimizer was used with a learning rate of 1×10^{-4} and the dice loss function and a weight decay configuration of 5×10^{-2} .

III. RESULTS AND DISCUSSION

A. Generation

Having started with S2-L2A data as input to the TerraMind model, Fig. 1 shows the qualitative evaluation of the generation output, whilst Table I shows the quantitative performance for ESRI LULC generation for the Karukinka study area. Overall, the model achieved a weighted intersection over union (IoU) score of 78.82%, which indicates strong agreement between the LULC classes generated by the model and the ESRI ground truth that we were comparing it against. Moreover, the model performed strongly in generating vegetation classes, namely trees (90%), and rangelands (87%). Bare ground and flooded vegetation came in fourth and fifth with F1-scores of 50% and 48% respectively. In respect to Figure 1, the rangeland class overlaps well with the presence of peatlands, but struggles to separate from other herbaceous vegetation.

TABLE I: Performance evaluation from TerraMind generation.

Classes	Support	F1-score
Water	13743498	0.99
Trees	31735327	0.90
Flooded vegetation	826811	0.50
Crops	3140	0
Built area	2231	0.13
Bare ground	1243421	0.48
Snow/ice	2612880	0.02
Clouds	5002	0
Rangeland	33721962	0.87

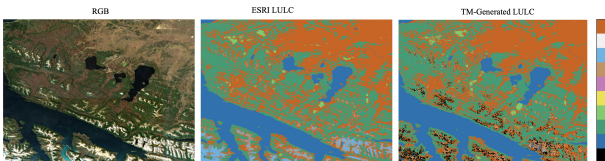


Fig. 1: Generated LULC map of the Karukinka region using TerraMind.

B. Forest traits mapping

The results shown in Table II and III, indicate superior performance of GFMs for both canopy density and leaf mapping, with both out performing ResNet by at least 20%. TerraMind was the best performing model, followed closely by Prithvi in both experiments. Fig 2 and 3 are qualitative evaluations of the canopy cover density and leaf form segmentation tasks respectively. The figures illustrate how Prithvi and TerraMind outperform ResNet in both segmentation tasks.

We can see that while the models where fine-tuned with coarse-grained targets, they were able to capture the spatio-spectral dimensions of the inputs and targets. We note that ViT based models (Prithvi and TerraMind) outperformed the ResNet.

TABLE II: Performance evaluation of ResNet, Prithvi and TerraMind on canopy cover density mapping.

Model	F1-score	IoU per Class		
		Other	Open	Closed
ResNet	0.54	0.38	0.47	0.17
Prithvi	0.74	0.58	0.68	0.40
TerraMind	0.75	0.58	0.69	0.41

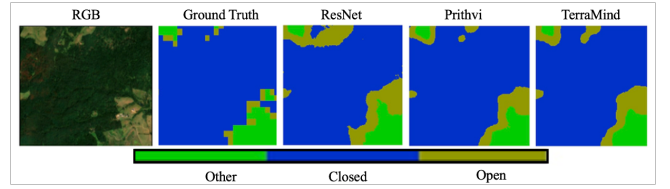


Fig. 2: Visual comparison of canopy cover density prediction by ResNet, Prithvi and TerraMind.

TABLE III: Performance evaluation of ResNet, Prithvi, and TerraMind on leaf form mapping.

Model	F1-score	IoU per class				
		Other	Needle leaf	Broad leaf	Mixed forests	Unknown forests
ResNet	0.41	0.42	0.21	0.17	0.03	0.18
Prithvi	0.67	0.56	0.43	0.56	0.33	0.42
TerraMind	0.70	0.63	0.55	0.52	0.42	0.43

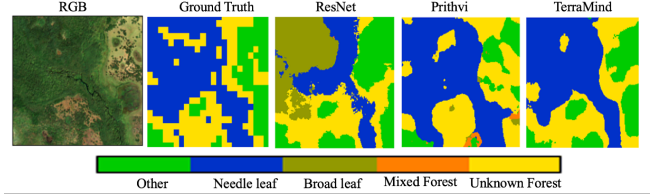


Fig. 3: Visual comparison of Leaf form prediction by ResNet, Prithvi and TerraMind.

C. Peatland detection

Figure 4 illustrates the three labels datasets derived in section II-D2 for fine-tuning of the GFMs. The COP 2020 LULC labels, overlap well with the presence of the peat moss. However, none of the input modalities except the RGB, can effectively distinguish between different subclasses of vegetation, such as distinguishing between peat moss and other herbaceous vegetation. This is even more pronounced for the Chilean LULC labels, where only certain red-brownish patches (signifying the presence of peat moss) are labelled as peatlands. The PEATGRIDS-NDVI labels align well with the presence of peat moss, and avoid labelling the north east section as peats. However, the coarseness of the original PEATGRIDS dataset, introduces artefacts that

prevent the accurate delineation of boundaries.



Fig. 4: Comparison of the three labels datasets derived for peatlands detection. Labels shown in yellow.

Table IV illustrates the performance of the three models. For the unimodal experiments, Prithvi and TerraMind outperform the ResNet model across all label datasets. The multimodal experiments with TerraMind produce superior performance in separating the peats from non-peats. Perhaps owing to the inclusion of S1, NDVI and DEM, which may help distinguish peatlands from other vegetation classes. Nonetheless, the Chilean LULC labels are the most challenging to reproduce.

TABLE IV: Performance evaluation of ResNet, Prithvi and TerraMind on peatland detection.

Model	Labels	F1-score	IoU per Class	
			Other	Peatland
ResNet	COP 2020 LULC	0.86	0.84	0.44
	PEATGRIDS-NDVI	0.59	0.66	0.10
	CHILEAN-LULC	0.90	0.89	0.10
Prithvi	COP 2020 LULC	0.90	0.88	0.60
	PEATGRIDS-NDVI	0.81	0.81	0.59
	CHILEAN-LULC	0.91	0.91	0.17
TerraMind	COP 2020 LULC	0.89	0.87	0.57
	PEATGRIDS-NDVI	0.88	0.84	0.67
	CHILEAN-LULC	0.92	0.92	0.19
TerraMind (multimodal)	COP 2020 LULC*	0.90	0.82	0.77
	CHILEAN-LULC	0.95	0.95	0.34

*Uses S2-L2A, NDVI, and DEM modality only.

Lastly, Figure 5 illustrates the predictions for the most performance model for each label dataset. Assuming the presence of peat moss (reddish-brown patches) to be the intuitive target, models produced using the COP 2020 LULC produce a high degree of false positives. On the other hand, the PEATGRIDS-NDVI and Chilean LULC has fewer false positives and a high degree of false negatives. We attribute this to the fact that none of the models are pretrained on data that represent subsurface dynamics, such as the presence of a peat layer, carbon content, or subsurface hydrodynamics.

IV. CONCLUSION

The results for the experiments illustrate moderate performance for the various use cases, when compared to the

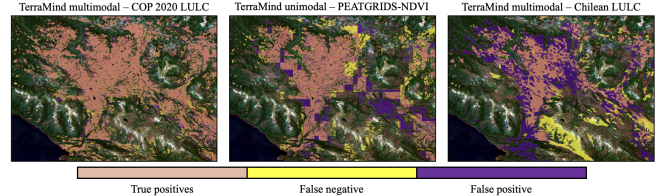


Fig. 5: Error map of peatland predictions over groundtruth for three experiments

general SOTA currently [32–35]. While this is true across the board, it is clear that the GFMs produce superior performance compared to the baseline ResNet models. Pretraining GFMs on earth observation data is the primary value of GFMs, because they address the domain-gap which often is the cause of low performance when using non-geospatial backbones such as ResNet for geospatial applications. The marginally higher performance of TerraMind over Prithvi is attributed to the fact that Prithvi was pretrained on 6 HLS bands while TerraMind was pretrained on all 12 S2-L2A bands. However, with the addition of supplementary modalities, TerraMind significantly outperforms the unimodal counterparts.

Consideration should also be given to the quality of the input data, in the context of model performance. While not shown in this paper, the performance of the models vary significantly when using single date satellite acquisitions versus temporal aggregates. Temporal bias is also evident in model predictions. In-addition, the nominal resolution of the input data (10m) coupled with the inability of transformers to recover pixel-level details, reduces the ability to detect small scale features or changes in vegetation. In this case, the models may benefit from high resolution inputs. Furthermore, depending on the region (persistent cloud cover), the consistent use of either temporal aggregates or unprocessed single time acquisition, should be considered. Ideally, multi-temporal sampling when creating fine-tuning datasets should be considered.

From the label data perspective, the resolution and ambiguity of the labels, significantly affect model performance. For example, the COP 2019 labels used in the forest traits mapping, are roughly at a 100m, which do not accurately delineate the boundaries between classes. This reduces the validity of the model assessment. Caution should thus be given, when using "off-the-shelf" datasets as labels, especially when initially derived through machine learning techniques. While not always possible, preference should be given to label datasets derived from field based observation, and corroborated by experts. Here the models may benefit from high fidelity hand-picked labels.

ACKNOWLEDGMENT

This work was supported by the MIT-IBM Watson AI Lab and Goldman Sachs.

REFERENCES

[1] D. Szwarcman, S. Roy, P. Fraccaro, T. E. Gíslason, B. Blumenstiel, R. Ghosal, P. H. De Oliveira, J. L. de Sousa Almeida, R. Sedona, Y. Kang *et al.*, “Prithvi-eo-2.0: A versatile multi-temporal foundation model for earth observation applications,” *IEEE Transactions on Geoscience and Remote Sensing*, 2025.

[2] J. Jakubik, F. Yang, B. Blumenstiel, E. Scheurer, R. Sedona, S. Maurogiovanni, J. Bosmans, N. Dionelis, V. Marsocci, N. Kopp *et al.*, “Terramind: Large-scale generative multimodality for earth observation,” *arXiv preprint arXiv:2504.11171*, 2025.

[3] Y. Cong, S. Khanna, C. Meng, P. Liu, E. Rozi, Y. He, M. Burke, D. Lobell, and S. Ermon, “Satmae: Pre-training transformers for temporal and multi-spectral satellite imagery,” *Advances in Neural Information Processing Systems*, vol. 35, pp. 197–211, 2022.

[4] S. Soni, A. Dudhane, H. Debary, M. Fiaz, M. A. Munir, M. S. Danish, P. Fraccaro, C. D. Watson, L. J. Klein, F. S. Khan *et al.*, “Earthdial: Turning multi-sensory earth observations to interactive dialogues,” in *Proceedings of the Computer Vision and Pattern Recognition Conference*, 2025, pp. 14 303–14 313.

[5] A. Fuller, K. Millard, and J. Green, “Croma: Remote sensing representations with contrastive radar-optical masked autoencoders,” *Advances in Neural Information Processing Systems*, vol. 36, pp. 5506–5538, 2023.

[6] Z. Xiong, Y. Wang, F. Zhang, A. J. Stewart, J. Hanna, D. Borth, I. Papoutsis, B. L. Saux, G. Camps-Valls, and X. X. Zhu, “Neural plasticity-inspired multimodal foundation model for earth observation,” *arXiv preprint arXiv:2403.15356*, 2024.

[7] M. Mendieta, B. Han, X. Shi, Y. Zhu, C. Chen, and M. Li, “Gfm: Building geospatial foundation models via continual pretraining,” *arXiv preprint arXiv:2302.04476*, vol. 3, 2023.

[8] U. Mall, C. P. Phoo, M. K. Liu, C. Vondrick, B. Hariharan, and K. Bala, “Remote sensing vision-language foundation models without annotations via ground remote alignment,” *arXiv preprint arXiv:2312.06960*, 2023.

[9] J. Cavender-Bares, F. D. Schneider, M. J. Santos, A. Armstrong, A. Carnaval, K. M. Dahlin, L. Fatoyinbo, G. C. Hurt, D. Schimel, P. A. Townsend *et al.*, “Integrating remote sensing with ecology and evolution to advance biodiversity conservation,” *Nature Ecology & Evolution*, vol. 6, no. 5, pp. 506–519, 2022.

[10] G. Mai, W. Huang, J. Sun, S. Song, D. Mishra, N. Liu, S. Gao, T. Liu, G. Cong, Y. Hu *et al.*, “On the opportunities and challenges of foundation models for geospatial artificial intelligence,” *arXiv preprint arXiv:2304.06798*, 2023.

[11] L. Yang, N. Chen, J. Yue, Y. Liu, J. Ma, P. Ghamisi, A. Plaza, and L. Fang, “Survey of multimodal geospatial foundation models: Techniques, applications, and challenges,” *arXiv preprint arXiv:2510.22964*, 2025.

[12] A. Xiao, W. Xuan, J. Wang, J. Huang, D. Tao, S. Lu, and N. Yokoya, “Foundation models for remote sensing and earth observation: A survey,” *IEEE Geoscience and Remote Sensing Magazine*, 2025.

[13] W. Zhang, J. Han, Z. Xu, H. Ni, H. Liu, and H. Xiong, “Towards urban general intelligence: A review and outlook of urban foundation models,” *arXiv preprint arXiv:2402.01749*, 2024.

[14] M. Mendieta, B. Han, X. Shi, Y. Zhu, and C. Chen, “Towards geospatial foundation models via continual pretraining,” in *Proceedings of the IEEE/CVF International Conference on Computer Vision*, 2023, pp. 16 806–16 816.

[15] P. Ghamisi, W. Yu, X. Zhang, A. Rizaldy, J. Wang, C. Zhou, R. Gloaguen, and G. Camps-Valls, “Geospatial foundation models to enable progress on sustainable development goals,” *arXiv preprint arXiv:2505.24528*, 2025.

[16] K. Janowicz, G. Mai, W. Huang, R. Zhu, N. Lao, and L. Cai, “Geofm: how will geo-foundation models reshape spatial data science and geoai?” *International Journal of Geographical Information Science*, vol. 39, no. 9, pp. 1849–1865, 2025.

[17] National Ecological Observatory Network, “Explore Field Sites,” <https://www.neonscience.org/field-sites/explore-field-sites>, accessed: 2026-01-17.

[18] WCS, “Positive Efforts by Region,” <https://www.wcs.org/our-work/wcs-high-integrity-peatlands-cross-regional-initiative/stories>, accessed: 2026-01-17.

[19] S. van Bellen, D. Mauquoy, P. D. M. Hughes, T. P. Roland, T. J. Daley, N. J. Loader, F. A. Street-Perrott, E. M. Rice, V. A. Pancotto, and R. J. Payne, “Late-holocene climate dynamics recorded in the peat bogs of tierra del fuego, south america,” *The Holocene*, vol. 26, no. 2, p. 253–265, 2016.

[20] K. He, X. Zhang, S. Ren, and J. Sun, “Deep residual learning for image recognition,” in *Proceedings of the IEEE conference on computer vision and pattern recognition*, 2016, pp. 770–778.

[21] C. Gomes, B. Blumenstiel, J. L. de Sousa Almeida, P. H. de Oliveira, P. Fraccaro, F. M. Escofet, D. Szwarcman, N. Simumba, R. Kienzler, and B. Zadrozny, “Terratorch: The geospatial foundation models toolkit,” 2025.

[22] ESA, “Copernicus sentinel-2 collection 1 msi level-2a (l2a),” 2021, accessed: 06.01.2026. [Online]. Available: <https://sentinels.copernicus.eu/sentinel-data-access/sentinel-products/sentinel-2-data-products/collection-1-level-2a>

[23] ESA, “Sentinel-1,” 2021, accessed: 06.01.2026. [Online]. Available: <https://documentation.dataspace.copernicus.eu/Data/SentinelMissions/Sentinel1.html#sentinel-1-level-1-ground-range-detected-grd>

[24] Copernicus, “Copernicus dem - global and european digital elevation model,” 2021, accessed: 06.01.2026. [Online]. Available: <https://dataspace.copernicus.eu/explore-data/data-collections/copernicus-contributing-missions/collections-description/COP-DEM>

[25] European Union’s Copernicus Land Monitoring Service, “Land cover 2015–2019 (raster 100 m), global, yearly – version 3,” 2025, accessed: 06.01.2026. [Online]. Available: <https://land.copernicus.eu/en/products/global-dynamic-land-cover/copernicus-global-land-service-land-cover-100m-collection-3\epoch-2015-2019-globe>

[26] EU-CLMS, “LCM-10,” 2025, accessed: 06.01.2026. [Online]. Available: <https://land.copernicus.eu/en/products/global-dynamic-land-cover/land-cover-2020-raster-10-m-global-annual>

[27] Forest Ecosystem Monitoring Department, “Change monitoring, cartographic correction, and updating of the inventory of native vegetation resources in the magallanes and chilean antarctic region,” 2020, accessed: 06.01.2026. [Online]. Available: <https://sit.conaf.cl/>

[28] M. T. Widayastuti, B. Minasny, J. Padarian, and F. Maggi, “Peatgrids: Mapping global peat thickness and carbon stock via digital soil mapping approach, dataset,” Nov 2024, accessed: 06.01.2026. [Online]. Available: <https://doi.org/10.5281/zenodo.15070037>

[29] T. G. Anderson, D. A. Christie, R. O. Chávez, M. Olea, and K. J. Anchukaitis, “Spatiotemporal peatland productivity and climate relationships across the western south american altiplano,” *Journal of Geophysical Research: Biogeosciences*, vol. 126, no. 6,

p. e2020JG005994, 2021, e2020JG005994 2020JG005994. [Online]. Available: <https://agupubs.onlinelibrary.wiley.com/doi/abs/10.1029/2020JG005994>

[30] R. O. Chávez, D. A. Christie, M. Olea, and T. G. Anderson, “A multiscale productivity assessment of high andean peatlands across the chilean altiplano using 31 years of landsat imagery,” *Remote Sensing*, vol. 11, no. 24, 2019. [Online]. Available: <https://www.mdpi.com/2072-4292/11/24/2955>

[31] ESRI, “10m annual land use land cover (9-class) v2,” 2025, accessed: 06.01.2026. [Online]. Available: <https://planetarycomputer.microsoft.com/dataset/io-lulc-annual-v02>

[32] M. S. R. Saimun and M. M. Rahman, “A comprehensive review of tree cover mapping using satellite sensor data,” *Discover Geoscience*, vol. 3, no. 1, p. 90, Aug 2025. [Online]. Available: <https://doi.org/10.1007/s44288-025-00201-x>

[33] J. Li, Y. Cai, Q. Li, M. Kou, and T. Zhang, “A review of remote sensing image segmentation by deep learning methods,” *International Journal of Digital Earth*, vol. 17, no. 1, p. 2328827, 2024. [Online]. Available: <https://doi.org/10.1080/17538947.2024.2328827>

[34] X. ZHANG, Q. SHI, Y. SUN, J. HUANG, and D. HE, “The review of land use/land cover mapping ai methodology and application in the era of remote sensing big data,” *Journal of Geodesy and Geoinformation Science*, vol. 7, no. 3, pp. 1–23, 2024. [Online]. Available: <https://www.scioopen.com/article/10.11947/j.JGGS.2024.0301>

[35] K. Cheng, C. Zhang, Y. Fan, H. Diao, and S. Xia, “Ai-based approaches for wetland mapping and classification: A review of current practices and future perspectives,” *Artificial Intelligence in Geosciences*, vol. 6, no. 2, p. 100165, 2025. [Online]. Available: <https://www.sciencedirect.com/science/article/pii/S2666544125000619>